Intelligent Automation And Soft Computing, 2018

Vol. 24,no. 3,623–631

Intelligent Control for Integrated Guidance and Control based on the Intelligent Characteristic Model

Jun Zhou, Zhenzhen Ge

Institute of Precision Guidance and Control, Northwestern Polytechnical University, Xi'an, China

ABSTRACT

In this paper, an adaptive integrated guidance and control (IGC) scheme for the homing missile is proposed based on the novel continuous characteristic model and the dynamic surface control technique. The novel continuous characteristic model is first proposed in the presence of unknown model coefficients and uncertainties. Then, the dynamic surface control technique is applied to the continuous characteristic model. The proposed IGC scheme guarantees the line-of-sight angular rates converge to an arbitrarily small neighbourhood of zero and all the closed-loop signals to be semi-globally uniformly ultimately bounded, which is proven using the Lyapunov stability theory. Finally, the effectiveness of the adaptive IGC scheme is demonstrated using nonlinear numerical simulations for the maneuvering target.

KEY WORDS: Integrated guidance and control, Intelligent control, Continuous characteristic model, Adaptive control, Dynamic surface control, Homing missile

1 INTRODUCTION

TRACTICAL missiles by virtue of their mission objectives, demand extremely accurate performance from their guidance and control components. The traditional design method of the missile guidance and control system is to design the guidance and control subsystems separately and then integrate them. As it ignores the coupling and time lag existing inevitably in the guidance and control subsystems, guidance and control subsystems fail to work synergistically, and the performance of overall missile system is not fully exploited (Yan & Ji, 2012). Considering these drawbacks in timescale separation design, integrated guidance and control (IGC) has been a hot topic of research in recent years (Wang & Wang, 2014). The IGC views the guidance subsystem and control subsystem as a whole and directly generates the fin deflection commands. Until now, a variety of approaches have been employed to design IGC laws, for example, feedback linearization (Menon et al., 2004), state dependent Riccati equation (Vaddi et al., 2009), active disturbance rejection control (Zhang & Wu, 2016), model predictive static programming (Padhi et al., 2014), sliding mode control (Song & Zhang, 2016), backstepping (Yan et al., 2014) and dynamic surface control (DSC) (Hou et al., 2013; Wang et al., 2015).

It is noted that most of the existing relevant literature on IGC designs assumed the involved model coefficients related to the missile-target range R or the relative velocity along the line of sight (LOS) $\dot{R}$ were known and accessible, and hence, all state variables were available to the control law. However, this assumption is quite restrictive and unreasonable in many applications, especially for the missile equipped with the infrared seeker or passive radar seeker. Furthermore, attack and sideslip angles are usually regarded as part of state variables in many works, whereas they are difficult to measure. Thus, only a subset of state variables is measurable and available to the control law. In this work, we mainly focus on the IGC design when all the involved model coefficients, unmatched uncertainties and states except for the system output are unknown and unavailable to the IGC law. Therefore, a second-order continuous characteristic model is first presented to reconstruct the original system based on the principle that the original system and its continuous characteristic model should have the same output when their inputs are equivalent.

A characteristic model has the following features. 1) It should be equivalent to its practical plant in output for the same input. 2) It compresses high-order terms, uncertainties and disturbances into several parameters without losing any information. In the

CONTACT Zhenzhen Ge gezhenzhen_nwpu@163.com

1990s, an integrated and practical all-coefficient adaptive control theory and method based on characteristic models were proposed (Wu et al., 2007). This control theory is independent of the original system model and has already been applied to many fields successfully (Zhang & Hu, 2012; Huang & Zhang, 2015). However, it is denoted by a slow time-varying second-order difference equation and requires that the sample time should be small enough to make the coefficients of the difference equation slow time-varying. The model mismatch and the truncation error between the discrete controller and the continuous system are inevitable. To eliminate these shortcomings, a continuous characteristic model is presented in this work. As the novel characteristic model has no truncation error and is not related to the sample time, its characteristic parameters vary much faster. On the account of this fact, the continuous characteristic model is incorporated with the robust adaptive dynamic surface control technique. To avoid the problem of explosion of complexity of the back-stepping method (Dimirovski et al., 2006), the DSC technique was proposed by introducing a first-order low pass filter at each design step. It has been extensively researched in many applications ranging from linear systems, nonlinear systems and stochastic systems (Wang & Lin, 2010; Kendrick et al., 2013; Song et al., 2014).

In this paper, we consider the IGC design for the homing missile based on the novel continuous characteristic model and the adaptive dynamic surface control approach in the presence of unknown model coefficients, uncertainties and intermediate state variables. The rest of this paper is organized as follows: In Section 2, the integrated guidance and control design for the pitch channel is introduced, for example, the original pitch channel dynamics model description, continuous characteristic model, design objective, IGC law design procedure and stability analysis. In Section 3, the integrated guidance and control design for the yaw and roll channels are presented. Simulations on the nonlinear missile model are conducted, and conclusions are drawn in Section 4 and 5, respectively.

2 INTEGRATED GUIDANCE AND CONTROL DESIGN FOR THE PITCH CHANNEL

2.1 Continuous Characteristic Model of the Pitch Channel

THE pitch channel model for the missile integrated guidance and control loop is given by (Liang et al., 2015).

$$\begin{cases} \dot{x}_1 = a_{11}x_1 + a_{12}x_2 + \Delta_1 \\ \dot{x}_2 = a_{22}x_2 + x_3 + \Delta_2 \\ \dot{x}_3 = a_{32}x_2 + b_3u + \Delta_3 \\ y = x_1 \end{cases} \tag{1}$$

Where $x_1 = \dot{\varepsilon}$, $x_2 = \alpha$ and $x_3 = \omega_z$ are the system states; $u = \delta_z$ and $y = \dot{\varepsilon}$ are the system input and output; Δ_1, Δ_2 and Δ_3 are the system uncertainties; $b_3 = QSLm_z^{\delta_z} / J_z$, $a_{11} = -2\dot{R}/R$, $a_{12} = -QSc_y^{\alpha} / mR$, $a_{22} = -QSc_y^{\alpha} / mV$ and $a_{32} = QSLm_z^{\alpha} / J_z$ are the model coefficients; m is the mass of the missile; V is the velocity of the missile; S and L are the reference area and length; R is the missile-target range; ε is the elevation angle of LOS; α is the attack angle; ω_z is the body-axis pitch rate; $Q = \rho V^2 / 2$ is the dynamic pressure; ρ is the air density; δ_z is the elevator deflection; J_z is the pitch moment of inertia; c_y^{α} is the partial derivative of lift force coefficient with respect to α; m_z^{α} and $m_z^{\delta_z}$ are the partial derivatives of pitching moment coefficient with respect to α and δ_z, respectively.

Remark 1. In general, c_y^{α} and $m_z^{\delta_z}$ are usually positive and negative constants, respectively. Hence, there exist two constants $\bar{a} < 0$ and $\bar{b} < 0$ such that $a_{12} \le \bar{a} < 0$ and $b_3 \le \bar{b} < 0$.

So far, a great variety of literature deals with IGC designs on the condition that all the involved model coefficients are known and available, whilst only the uncertainties are unknown. Actually, for many missiles equipped with the infrared seeker or passive radar seeker, the model coefficients related to R or $\dot{R}$ are unknown and unavailable. So, the restrictive assumption in previous works is unreasonable in many cases. As a result, in this paper, it is assumed that the model coefficients and uncertainties of model (1) satisfy the following assumption instead of the restrictive one.

Assumption 1. All the involved model coefficients and uncertainties of model (1) are unknown bounded time-varying functions with bounded derivatives, and all the bounds are also unknown.

At present, in some literature, the system states are considered to be known and available. But the attack and sideslip angles are difficult to measure. To solve the problem, the model states are supposed to meet the following assumption.

Assumption 2. Only the system input u and output y are available for measurement.

Due to Assumption 1 and Assumption 2, it is of great interest to conduct an IGC design without a state observer and the designed adaptive law should be

much simple. In order to achieve this objective, a novel continuous characteristic model denoted by a second-order continuous time-varying differential equation is proposed. For the same input, the continuous characteristic model has the same output as that of its original model. As the proposed IGC design only uses the system output, it is able to substitute the continuous characteristic model for its original model in the design process. The novel continuous characteristic model of original model (1) is presented as follows.

According to (1), the first-order derivative of output is

$$\dot{x}_1 = a_{11}x_1 + a_{12}x_2 + \Delta_1 \tag{2}$$

Then, the third-order derivative of output is expressed as

$$\begin{aligned}\dddot{x}_1 = {} & a_{11}\ddot{x}_1 + 2\dot{a}_{11}\dot{x}_1 + \ddot{a}_{11}x_1 + \\ & a_{12}\ddot{x}_2 + 2\dot{a}_{12}\dot{x}_2 + \ddot{a}_{12}x_2 + \ddot{\Delta}_1\end{aligned} \tag{3}$$

From (1), we have

$$\ddot{x}_2 = a_{22}\dot{x}_2 + (\dot{a}_{22} + a_{32})x_2 + b_3u + \dot{\Delta}_2 + \Delta_3 \tag{4}$$

Substituting (4) into (3) results to

$$\begin{aligned}\dddot{x}_1 = {} & a_{11}\ddot{x}_1 + \ddot{a}_{11}x_1 + a_{12}a_{22}\dot{x}_2 + \ddot{a}_{12}x_2 + \ddot{\Delta}_1 + \\ & a_{12}[(\dot{a}_{22} + a_{32})x_2 + b_3u + \dot{\Delta}_2 + \Delta_3]\end{aligned} \tag{5}$$

According to (2), it can be obtained that

$$x_2 = (\dot{x}_1 - a_{11}x_1 - \Delta_1)/a_{12} \tag{6}$$

Substituting (6) into (5) results to

$$\dddot{x}_1 + q_2\ddot{x}_1 + q_1\dot{x}_1 + q_0x_1 = bu + w \tag{7}$$

where q_2 , q_1 , q_0 , b and w are time-varying functions, and their expressions are presented as follows:

$$q_2 = -\left(a_{11} + a_{22} + 2\dot{a}_{12}/a_{12}\right) \tag{8}$$

$$\begin{aligned}q_1 = {} & -2\dot{a}_{11} - \dot{a}_{22} - a_{32} - \ddot{a}_{12}/a_{12} + a_{11}a_{22} + \\ & \left(a_{22}\dot{a}_{12} + 2a_{11}\dot{a}_{12} + 2\dot{a}_{12}^2\right)/a_{12}^2\end{aligned} \tag{9}$$

$$\begin{aligned}q_0 = {} & -\ddot{a}_{11} + a_{11}\dot{a}_{22} + a_{11}a_{32} - 2a_{11}\dot{a}_{12}^2/a_{12}^2 - \\ & \left(a_{22}a_{11}\dot{a}_{12} - 2\dot{a}_{11}\dot{a}_{12} - a_{11}\ddot{a}_{12}\right)/a_{12} + \dot{a}_{11}a_{22}\end{aligned} \tag{10}$$

$$b = a_{12}b_3 \tag{11}$$

$$\begin{aligned}w = {} & \ddot{\Delta}_1 - \frac{a_{12}a_{22} + 2\dot{a}_{12}}{a_{12}}\dot{\Delta}_1 + a_{12}\dot{\Delta}_2 + a_{12}\Delta_3 + \\ & \left[\frac{a_{22}\dot{a}_{12} - \ddot{a}_{12}}{a_{12}} + \frac{2\dot{a}_{12}^2}{a_{12}^2} - \dot{a}_{22} - a_{32}\right]\Delta_1\end{aligned} \tag{12}$$

As $y = x_1$, from (7), one can obtain that

$$\dddot{y} + q_1\ddot{y} + q_0\dot{y} = bu + \xi \tag{13}$$

where $\xi = w - \dddot{y} + \left(1 - q_2\right)\ddot{y}$.

Let $\delta > 1$ is a positive constant arbitrarily, then define

$$\begin{aligned}&\upsilon_1 = \frac{\dot{y}}{\dot{y}^2 + y^2 + \delta}\ ,\ \upsilon_2 = \frac{y}{\dot{y}^2 + y^2 + \delta}, \\ &\upsilon_3 = \frac{\delta}{\dot{y}^2 + y^2 + \delta}\ ,\ \ \zeta = \sum_{i=0}^{m}\upsilon_3^i.\end{aligned} \tag{14}$$

where $m > 0$ is a positive integer. Then, the compress mapping function f_s is defined as

$$f_s = \zeta\upsilon_1\ddot{y} + \zeta\upsilon_2\dot{y} + \upsilon_3^{m+1}y \tag{15}$$

Note that the compress mapping function has the property that $f_s = 1$. Combining (15) with (13), obviously, it can be obtained that

$$\begin{aligned}&\dddot{y}(t) + a_1(t)\ddot{y}(t) + a_0(t)\dot{y}(t) \\ &= b_0(t)u(t) + d(t)\end{aligned} \tag{16}$$

where a_1 , a_0 , b_0 and d are time-varying functions, and their expressions are presented as follows:

$$\begin{aligned}&a_1(t) = q_1 - \zeta\upsilon_1\xi, \\ &a_0(t) = q_0 - \zeta\upsilon_2\xi, \\ &b_0(t) = b, \\ &d(t) = \upsilon_3^{m+1}\xi.\end{aligned} \tag{17}$$

In summary, equation (16) is called the continuous characteristic model of system (1), a_1 , a_0 , b_0 and d are the time-varying characteristic parameters. Moreover, from the above theoretical deduction, it has been proven that the continuous characteristic model has the same output as that of its original model for the same input.

Remark 2. There are many choices for the intermediate parameters δ and m appearing in (14), that is, the compress mapping function is not unique. It means that the original system has many continuous characteristic models with different characteristic parameters. The main purpose of above deduction is to prove the existence of continuous characteristic model, which is the most important of all for the IGC design conducted in this paper. Due to the characteristic parameters that are related to the coefficients and uncertainties of model (1), which are supposed to be unknown in assumption 1, all the characteristic parameters are also unknown.

In addition, for the stability of the closed-loop system, the characteristic parameters are supposed to

satisfy the following reasonable assumption in view of their physical backgrounds.

Assumption 3. The characteristic parameters $a_1(t)$, $a_0(t)$, $b_0(t)$ and $d(t)$ are bounded time functions having bounded derivatives.

2.2 Design objective

The objective of IGC design can be elaborated as: Use the continuous characteristic model instead of its original model to design an IGC law in the presence of unknown model coefficients, mismatched uncertainties and states except the output of model, which should guarantee the missile intercepts the target with small miss distance and keep all the states of missile stable.

By accepting the concept that zeroing LOS angular rates will lead to a successful interception with zero miss distance, the specific guidelines for the IGC design are given as follows.

(1) To sustain LOS angular rates $\dot{\varepsilon}$ and $\dot{\eta}$ as zeros for making the miss distance small.

(2) To maintain the roll angle γ in a small neighbourhood of zero.

(3) To stabilize the states of the missile and be robust to the unknown coefficients and uncertainties existing in the missile dynamics.

2.3 IGC Law Design

As the characteristic model (16) is a fast time-varying linear system with a matched uncertainty, the adaptive dynamic surface control approach has been the most common method for such a kind of systems recently (Song et al., 2014). In this section, an adaptive dynamic surface control algorithm is developed to deal with the output control problem under Assumption 3.

The second-order continuous characteristic model (16) is written in the state-space form

$$\begin{cases} \dot{\boldsymbol{x}}(t) = \boldsymbol{A}(t)\boldsymbol{x}(t) + \boldsymbol{b}(t)u(t) + \boldsymbol{d}(t) \\ y(t) = x_1(t) \end{cases} \tag{18}$$

Where $u \in \mathrm{R}$ and $y \in \mathrm{R}$ are the system input and output, $\boldsymbol{x} = [x_1, x_2]^{\mathrm{T}} \in \mathrm{R}^2$ is the system state vector, and

$$\boldsymbol{A} = \begin{bmatrix} 0 & 1 \\ -a_0(t) & -a_1(t) \end{bmatrix},$$

$$\boldsymbol{b}(t) = \begin{bmatrix} 0 \\ b_0(t) \end{bmatrix}, \quad \boldsymbol{d}(t) = \begin{bmatrix} 0 \\ d(t) \end{bmatrix}.$$

Remark 3. Since $b_0(t) = b = a_{12}b_3$, meanwhile, $a_{12} \le \overline{a} < 0$ and $b_3 \le \overline{b} < 0$ in Remark 1, it can be seen that $b_0(t) > 0$ and the sign of $b_0(t)$ is known and constant throughout the engagement.

The robust output-feedback adaptive dynamic surface control design for system (18) is proceeded as follows:

Step 1: The first surface error is defined as

$$S_1 = y \tag{19}$$

By considering (18), the time derivative of first surface error is

$$\dot{S}_1 = \dot{y} = -c_1 S_1 + \left[(x_2 - \alpha_1) + \alpha_1 + c_1 S_1 \right] \tag{20}$$

where c_1 is a positive design parameter, α_1 is the virtual control to be designed to stabilize (20) in the absence of $(x_2 - \alpha_1)$.

Choosing the virtual control as

$$\alpha_1 = -c_1 S_1 \tag{21}$$

Let α_1 as the input of the following first-order filter.

$$\tau_2 \dot{x}_{2d} + x_{2d} = \alpha_1 \tag{22}$$

Where τ_2 is the time constant, x_{2d} is the filter output.

Step 2: The second surface error is defined as

$$S_2 = x_2 - x_{2d} = \dot{y} - x_{2d} \tag{23}$$

Whose time derivative is

$$\dot{S}_2 = -c_2 S_2 + b_0(t)\left[u + \boldsymbol{\theta}^{\mathrm{T}} \boldsymbol{\omega} \right] \tag{24}$$

Where c_2 is a positive design parameter, and

$$\begin{aligned} &\boldsymbol{\theta} = \left[1/b_0, -a_0/b_0, -a_1/b_0, -d/b_0 \right]^{\mathrm{T}}, \\ &\boldsymbol{\omega} = \left[c_2 S_2 - \dot{x}_{2d}, y, \dot{y}, 1 \right]^{\mathrm{T}}. \end{aligned} \tag{25}$$

Define the estimate error as

$$\tilde{\boldsymbol{\theta}} = \boldsymbol{\theta} - \hat{\boldsymbol{\theta}} \tag{26}$$

Where $\hat{\boldsymbol{\theta}}$ is the estimate of $\boldsymbol{\theta}$, and the adaptive law is defined as

$$\dot{\hat{\boldsymbol{\theta}}} = \boldsymbol{\Gamma} S_2 \boldsymbol{\omega} - \sigma \hat{\boldsymbol{\theta}} \tag{27}$$

Where $\boldsymbol{\Gamma}$ is a positive definite matrix, σ is a positive design parameter.

In final step, the actual system input is chosen as

$$u = -\hat{\boldsymbol{\theta}}^{\mathrm{T}} \boldsymbol{\omega} \tag{28}$$

Remark 4. It is seen that the design procedure is quite simple compared with traditional adaptive controllers for linear time-varying (LTV) plants. The number of estimate parameters is small and constant, which is not

related to the model order and relative degree of its original system. In addition, the proposed scheme does not need a state observer any more. Thus, the algorithm does not introduce state observer errors, which may affect the rate of convergence and the output error to some extent.

2.4 Stability Analysis

The stability analysis is based on the Lyapunov stability theory. First, define the boundary layer error as

$$y_1 = x_{2d} - \alpha_1 \tag{29}$$

In view of (22) and (29), we have

$$\begin{aligned} y_1\dot{y}_1 &= y_1\left[\left(\alpha_1 - x_{2d}\right)/\tau_2 - \dot{\alpha}_1\right] \\ &\le -y_1^2/\tau_2 + |y_1|\eta_1 \end{aligned} \tag{30}$$

Where η_1 is a positive continuous function. Similarly to the linear time-invariant case (Wang & Lin, 2010), the existence of η_1 can be checked with the Assumption 3.

Consider the following Lyapunov function candidate

$$V = \left[S_1^2 + S_2^2 + y_1^2 + b_0(t)\tilde{\boldsymbol{\theta}}^{\mathrm{T}}\boldsymbol{\Gamma}^{-1}\tilde{\boldsymbol{\theta}}\right]/2 \tag{31}$$

Where $\tilde{\boldsymbol{\theta}} = \boldsymbol{\theta} - \hat{\boldsymbol{\theta}}$ is the estimate errors vector. As mentioned in Remark 3, there exists a constant $\underline{b} > 0$ such that $b_0(t) \ge \underline{b} > 0$, thus V is positive definite.

Theorem 1: On condition that assumption 1-3 are satisfied, the closed-loop system consisting of the equivalent continuous characteristic model (16) instead of its original LTV system (1) in the design process, the control law(28), the adaptive update law (27) and the first-order filters (22) is considered. If the positive constant R_0 given arbitrarily meets the following inequality

$$V(0) \le R_0$$

there exist c_1, c_2, τ_2, $\boldsymbol{\Gamma}$ and σ to guarantee that all closed-loop signals are uniformly bounded and the output error S_1 is arbitrarily small with proper design parameters.

Proof

According to (27) - (30), the time derivative of (31) yields

$$\begin{aligned} \dot{V} \le& -c_1S_1^2 - c_2S_2^2 + \sigma b_0(t)\tilde{\boldsymbol{\theta}}^{\mathrm{T}}\boldsymbol{\Gamma}^{-1}\hat{\boldsymbol{\theta}} + \\ & S_1\left(S_2 + y_1\right) + \dot{b}_0(t)\tilde{\boldsymbol{\theta}}^{\mathrm{T}}\boldsymbol{\Gamma}^{-1}\tilde{\boldsymbol{\theta}}/2 + \\ & b_0(t)\tilde{\boldsymbol{\theta}}^{\mathrm{T}}\boldsymbol{\Gamma}^{-1}\dot{\boldsymbol{\theta}} + \left(-\frac{y_1^2}{\tau_2} + |y_1|\eta_1\right) \end{aligned} \tag{32}$$

Using Young's inequality, we have

$$\begin{aligned} &|y_1|\eta_1 \le \frac{y_1^2\eta_1^2}{2\varepsilon} + \frac{\varepsilon}{2}, \\ &\tilde{\boldsymbol{\theta}}^{\mathrm{T}}\boldsymbol{\Gamma}^{-1}\hat{\boldsymbol{\theta}} \le -\frac{1}{2}\tilde{\boldsymbol{\theta}}^{\mathrm{T}}\boldsymbol{\Gamma}^{-1}\tilde{\boldsymbol{\theta}} + \frac{1}{2}\boldsymbol{\theta}^{\mathrm{T}}\boldsymbol{\Gamma}^{-1}\boldsymbol{\theta}. \end{aligned} \tag{33}$$

Where ε is a positive constant given arbitrarily. According to (33), the inequality (32) is written as

$$\begin{aligned} \dot{V} \le& -c_1S_1^2 - c_2S_2^2 - \frac{1}{2}\sigma b_0(t)\tilde{\boldsymbol{\theta}}^{\mathrm{T}}\boldsymbol{\Gamma}^{-1}\tilde{\boldsymbol{\theta}} + \\ & \left(S_1^2 + \frac{S_2^2}{2} + \frac{y_1^2}{2}\right) + \frac{1}{2}\sigma b_0(t)\boldsymbol{\theta}^{\mathrm{T}}\boldsymbol{\Gamma}^{-1}\boldsymbol{\theta} + \\ & \frac{1}{2}\dot{b}_0(t)\tilde{\boldsymbol{\theta}}^{\mathrm{T}}\boldsymbol{\Gamma}^{-1}\tilde{\boldsymbol{\theta}} + b_0(t)\tilde{\boldsymbol{\theta}}^{\mathrm{T}}\boldsymbol{\Gamma}^{-1}\dot{\boldsymbol{\theta}} + \\ & \left(-\frac{1}{\tau_2} + \frac{\eta_1^2}{2\varepsilon}\right)y_1^2 + \frac{\varepsilon}{2} \end{aligned} \tag{34}$$

Define the function

$$\begin{aligned} \varphi =& \sigma b_0(t)\boldsymbol{\theta}^{\mathrm{T}}\boldsymbol{\Gamma}^{-1}\boldsymbol{\theta}/2 + b_0(t)\tilde{\boldsymbol{\theta}}^{\mathrm{T}}\boldsymbol{\Gamma}^{-1}\dot{\boldsymbol{\theta}} + \\ & \dot{b}_0(t)\tilde{\boldsymbol{\theta}}^{\mathrm{T}}\boldsymbol{\Gamma}^{-1}\tilde{\boldsymbol{\theta}}/2 + \varepsilon/2 \end{aligned} \tag{35}$$

Substituting (35) into (34) yields

$$\begin{aligned} \dot{V} \le& -c_1S_1^2 - c_2S_2^2 - \frac{1}{2}\sigma b_0(t)\tilde{\boldsymbol{\theta}}^{\mathrm{T}}\boldsymbol{\Gamma}^{-1}\tilde{\boldsymbol{\theta}} + \\ & \left(-\frac{1}{\tau_2} + \frac{\eta_1^2}{2\varepsilon}\right)y_1^2 + \left(S_1^2 + \frac{S_2^2}{2} + \frac{y_1^2}{2}\right) + \varphi \end{aligned} \tag{36}$$

Define the compact set

$$\Omega_0 := \left\{\left(S_1, S_2, y_1, \tilde{\boldsymbol{\theta}}\right) : V \le R_0\right\} \in \mathrm{R}^7 \tag{37}$$

Where R_0 is a given positive constant. Thus, from (37), the continuous functions η_1 and φ have maximums on Ω_0, say, M_1 and M_φ, respectively.

Choose

$$\begin{aligned} &c_1 \ge 1 + \alpha_0,\ c_2 \ge 0.5 + \alpha_0, \\ &1/\tau_2 \ge 0.5 + M_1^2/2\varepsilon + \alpha_0,\ \sigma \ge 2\alpha_0. \end{aligned} \tag{38}$$

Where α_0 is a positive design parameter.

Substituting the inequality (38) into (36), we obtain

$$\dot{V} \le -2\alpha_0 V + M_\varphi \tag{39}$$

Hence, if $R_0 \ge V(0)$ and α_0 is chosen as

$$\alpha_0 \ge M_\varphi/2R_0 \tag{40}$$

then $\dot{V} \le 0$ on $V = R_0$.

From the inequality (39), we can obtain that

$$0 \le V \le \left[V(0) - \frac{M_\varphi}{2\alpha_0} \right] e^{-2\alpha_0 t} + \frac{M_\varphi}{2\alpha_0} \tag{41}$$

Hence,

$$\lim_{t\to\infty} |S_1(t)| \le \lim_{t\to\infty} \left| \sqrt{2V(t)} \right| = \sqrt{M_\varphi / \alpha_0} \tag{42}$$

Therefore, the output error can be made arbitrarily small with a large value of α_0, which can be implemented by letting the values of c_1, c_2 and σ large enough and that of τ_2 small enough.

3 CONTROL DESIGN FOR THE YAW AND ROLL CHANNELS

SIMILARLY to the pitch channel, the yaw channel model for the integrated guidance and control loop is given by

$$\begin{cases} \dot{x}_1 = a_{11}x_1 + a_{12}x_2 + \Delta_1 \\ \dot{x}_2 = a_{22}x_2 + x_3 + \Delta_2 \\ \dot{x}_3 = a_{32}x_2 + b_3 u + \Delta_3 \\ y = x_1 \end{cases} \tag{43}$$

Where $x_1 = \eta$, $x_2 = \beta$ and $x_3 = \omega_y$ are system states; $x_1 = \eta$ is the azimuth angle of LOS; β is the sideslip angle; ω_y is the body-axis yaw rate; $u = \delta_y$ and $y = \dot{\eta}$ are system input and output; δ_y is the rudder deflection; Δ_1, Δ_2 and Δ_3 are uncertainties; $a_{11} = -2\dot{r}/r$, $a_{12} = QSc_z^\beta / mr$, $a_{22} = QSc_z^\beta / mV$, $a_{32} = QSLm_y^\beta / J_y$ and $b_3 = QSLm_y^{\delta_y} / J_y$ are model coefficients; J_y is the yaw moment of inertia; c_z^β is the partial derivative of side force coefficient with respect to β; m_y^β and $m_y^{\delta_y}$ are the partial derivatives of yawing moment coefficient with respect to β and δ_y, respectively.

Obviously, the yaw channel model (43) takes the form of the pitch channel model. Thus, their adaptive control algorithms are similar and the design procedure of yaw channel is omitted.

Additionally, the roll channel model is given by

$$\begin{cases} \dot{x}_1 = x_2 + \Delta_1 \\ \dot{x}_2 = b_2 u + \Delta_2 \\ y = x_1 \end{cases} \tag{44}$$

Where $x_1 = \gamma$ and $x_2 = \omega_x$ are the system states; γ is the roll angle; ω_x is the body-axis roll rate; $u = \delta_x$ and $y = \gamma$ are the system input and output; δ_x is the aileron deflection; Δ_1 and Δ_2 are systems uncertainties; $b_2 = QSLm_x^{\delta_x} / J_x$ is the model coefficient; J_x is the roll moment of inertia; $m_x^{\delta_x}$ is the partial derivative of rolling moment coefficient with respect to δ_x.

Although the roll channel model (44) is much different from the pitch and yaw channels, the proposed scheme is not related to the model structure. So, the adaptive control algorithm can be utilized to stabilize system (44) is given as follows, the form of which is same as that of the pitch and yaw channels.

$$\begin{cases} S_1 = y = \gamma \\ \alpha_1 = -c_1 S_1 \\ \tau_2 \dot{x}_{2d} + x_{2d} = \alpha_1 \\ S_2 = \dot{y} - x_{2d} \\ \dot{\hat{\boldsymbol{\theta}}} = \boldsymbol{\Gamma} S_2 \boldsymbol{\omega} - \sigma \hat{\boldsymbol{\theta}} \\ u = -\hat{\boldsymbol{\theta}}^{\mathrm{T}} \boldsymbol{\omega} \end{cases} \tag{45}$$

Where $\hat{\boldsymbol{\theta}}$ is the estimate of $\boldsymbol{\theta}$ defined in (25), $\boldsymbol{\omega}$ is defined in (25). The design parameters c_1, c_2, τ_2 and σ should satisfy the inequality (38).

4 SIMULATION RESULTS

IN this section, the effectiveness of the newly proposed IGC scheme based on the continuous characteristic and the dynamic surface control technique is verified through the 6DOF nonlinear numerical simulation (Wang et al., 2016), where an air-to-surface missile is considered in its terminal homing to intercept a maneuvering target on ground.

As the forms of IGC laws for pitch, yaw and roll channels are the same as each other, in this section, we select the same design parameters for each channel. The design parameters of the novel IGC law are chosen as

$$c_1 = 2,\ c_2 = 4,\ \tau_2 = 0.02,$$
$$\sigma = 1,\ \boldsymbol{\Gamma} = \mathrm{diag}\{2, 2, 2, 2\}.$$

and the initial value of $\hat{\boldsymbol{\theta}}$ is set as $[0, 0, 0, 0]^{\mathrm{T}}$.

For comparison, the traditional separate channel guidance and control scheme with proportional navigation guidance (PNG) plus proportional-integral-derivative (PID) control law is also carried out. For simplicity, the novel IGC law and traditional separate scheme are denoted as NIGC and TSGC, respectively.

In numerical simulations, the missile dynamics parameters are outlined in Table 1. c_{x0} is the zero-lift drag coefficient. c_x^α and c_x^β are the partial derivatives of drag force coefficient with respect to α and β, respectively. c_y^β and $c_y^{\delta_z}$ are partial derivatives of lift force coefficient with respect to β and δ_z, respectively. c_z^α and $c_z^{\delta_y}$ are partial derivatives of side force

coefficient with respect to α and δ_y, respectively. m_x^{α} and m_x^{β} are partial derivatives of rolling moment coefficient with respect to α and β, respectively. The initial states of the missile are respectively set as

$$V = 600\text{m/s}\,,\ \theta = \psi_v = 0\,,$$

$$\vartheta = \psi = 0.02\text{rad}\,,\ \gamma = 0.1\text{rad}\,,$$

$$\omega_x = 0.2\text{rad/s}\,,\ \omega_y = \omega_z = 0.1\text{rad/s}\,.$$

In the inertial coordinate system, the initial position of the missile is set as $[0, 10000, 0]^{\mathrm{T}}$ m . The initial position, velocity, and acceleration of the target in the inertial coordinate system are set as $[8000, 0, -2000]^{\mathrm{T}}$ m , $[-17, 0, 0]^{\mathrm{T}}$ m/s and $[-1.5, 0, -10\cos(0.5t)]^{\mathrm{T}}$ m/s^2 , respectively.

Table 1. The Nominal Parameters of Missile Dynamics.

Name	Value	Name	Value	Name	Value
m	1200 kg	m_x^{β}	-0.38	c_x^{β}	0.4
S	0.42 m^2	$m_x^{\delta_x}$	1.06	c_y^{α}	57.2
L	0.68 m	m_y^{β}	-27.3	c_y^{β}	-0.1
J_x	100 kg·m^2	$m_y^{\delta_y}$	-13.3	$c_y^{\delta_z}$	5.7
J_y	5700 kg·m^2	m_z^{α}	-28.2	c_z^{α}	0.1
J_z	5600 kg·m^2	$m_z^{\delta_z}$	-14.0	c_z^{β}	-56.3
ρ	1.16 kg/m^3	c_{x0}	0.2	$c_z^{\delta_y}$	-5.6
g	9.8 m/s^2	c_x^{α}	0.4	m_x^{α}	0.45

The NIGC and TSGC approaches will be conducted in the case. The curves of locations, LOS angular rates, aerodynamic angles and deflection angles are presented in the Figure 1~Figure 3. The three dimensional (3D) trajectory of the missile with respect to NIGC and TSGC is shown in Figure 1. The curves of missile-target range and LOS angular rates are presented in Figure 2. The missile distance of the NIGC is 0.1537m, while, the missile distance of the TSGC is 8.3206m. The proposed IGC law has smaller missile distance than the classical separate channel scheme, and can guarantee the missile hits the target with higher accuracy. In addition, it is known that the NIGC scheme has better transient response performance in driving LOS angular rates to zero than that of TSGC approach from Figure 2(b). The angle of attack, sideslip angle and velocity bank angle are shown in Figure 3(a), and the deflection angles of the roll, yaw, and pitch control surface are presented in Figure 3(b).

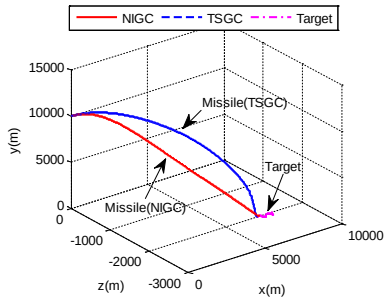

Figure 1. The Trajectory of the Missile.

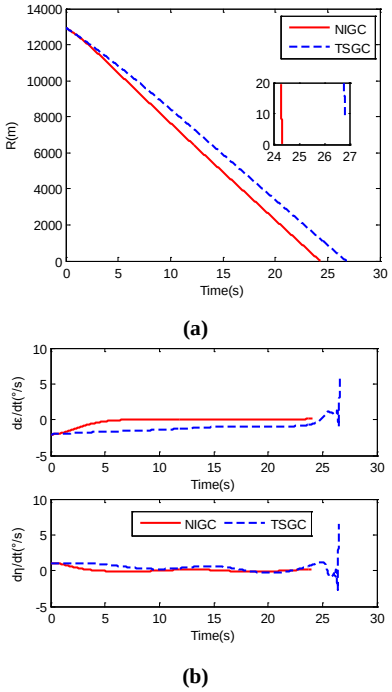

(a)

(b)

Figure 2. Simulation Results: (a) Missile-target Range; and (b) LOS Angular Rates.

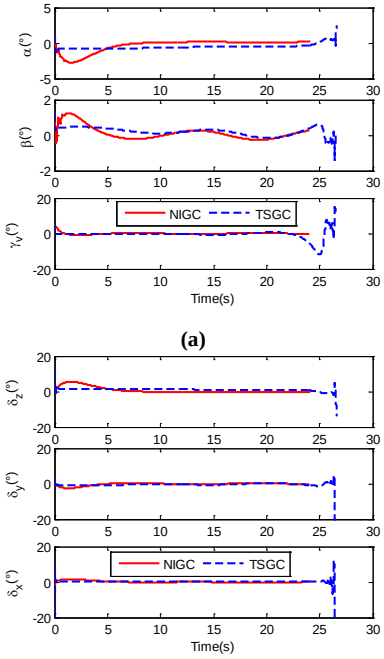

(a)

(b)

Figure 3. Simulation Results: (a) Angles α, β and γ_v; and (b) Fin Deflections δz, δy and δx.

According to Figure 2(b), for the TSGC scheme, LOS angular rates begin to diverge rather than converge to zero when the missile gets close to the target at the last moment. Meanwhile, it also makes the fin deflections increase largely and chatter, which affects the Euler angles and angular rates directly. But on the contrary, for the NIGC scheme, the LOS angular rates converge to a small neighbourhood of zero in finite time and do not diverge. Therefore, the missile distance of the NIGC scheme is much smaller than that of the TSGC scheme.

In order to verify the robustness of the IGC method, one hundred times of Monte Carlo simulations are conducted. Suppose that the coefficients of aerodynamics forces and moments all offset randomly by -20% ~ +20% of their respective nominal values. The impact point deviation distributions of the Monte Carlo simulations are shown in Figure 4.

The mean missile distance of the NIGC is 0.2343m with a standard deviation 0.1449m. However, the mean missile distance of the TIGC is 1.0685m with standard deviation of 0.8861m. As a result, it can be obtained that the proposed NIGC scheme is more robust to uncertainties and has better performance during the interception than the classical TSGC scheme.

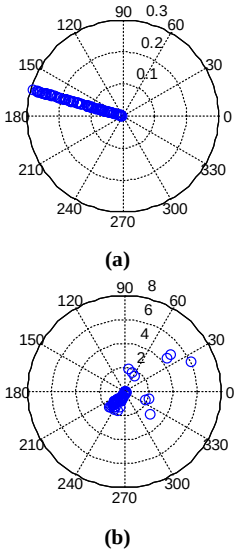

(a)

(b)

Figure 4. Impact Point Deviation Distributions: (a) NIGC and (b) TIGC.

5 CONCLUSION

A novel adaptive IGC scheme for the homing missile is proposed based on the novel fully continuous characteristic model of the IGC model and the dynamic surface control technique. The major advantages of the proposed IGC scheme are drawn as follows:

(1) For the IGC model of each channel, the continuous characteristic model is established for the IGC law design. The continuous characteristic model is equivalent to its original model in output, that is, their outputs are identical when their inputs are the same.

(2) With the novel continuous characteristic model, all the model coefficients of the IGC dynamics model related to the missile-target range, relative velocity along the LOS and aerodynamic coefficients can be unknown. Moreover, the intermediate states such as attack angle, sideslip angle and angular rates of roll, yaw and pitch are also unavailable for the proposed IGC law which only utilizes the LOS angular rates.

(3) The dynamic surface control method is used for the continuous characteristic model to drive the LOS angular rates to an arbitrarily small neighborhood of zero and guarantee the stability of the closed-loop system.

(4) Nonlinear numerical simulations explicitly demonstrate the effectiveness of the proposed IGC scheme, which has better performance than the classical separate channel guidance and control scheme.

6 ACKNOWLEDGMENT

THE authors would like to thank the reviewers for their constructive comments and suggestions.

7 DISCLOSURE STATEMENT

NO potential conflict of interest was reported by the authors.

8 REFERENCES

G.M. Dimirovski, Y.W. Jing, W.L. Li, & X.P. Liu. (2006). Adaptive back-stepping design of TCSC robust nonlinear control for power systems, *Intelligent Automation and Soft Computing*. 12(1), 75-87.

H. Huang, & Z. Zhang. (2015). Characteristic model-based H2/H∞ robust adaptive control during the re-entry of hypersonic cruise vehicles, *Science China Information Sciences*. 58(1), 012202.

M. Z. Hou, X.L. Liang, & G.R. Duan. (2013). Adaptive block dynamic surface control for integrated missile guidance and autopilot, *Chinese Journal of Aeronautics*. 26(3), 741-750.

A. S. Kendrick Y. Lin, & A.B. Waseem. (2013). Adaptive dynamic surface control for a class of MIMO nonlinear systems with actuator failures, *International Journal of Systems Science*. 44(3), 479-492.

X. L. Liang, M.Z. Hou, & G. R. Duan. (2015). Adaptive dynamic surface control for integrated missile guidance and autopilot in the presence of input saturation, *Journal of Aerospace Engineering*. 28(5), 04014121.

P. K. Menon, G. D. Sweriduk, E.J. Ohlmeyer, & D. S. Malyevac. (2004). Integrated guidance and control of moving mass actuated kinetic warheads, *Journal of Guidance Control and Dynamics*. 27(1), 118-126.

R. Padhi, C. Chawla, & P.G. Das. (2014). Partial integrated guidance and control of interceptors for high-speed ballistic targets, *Journal of Guidance Control and Dynamics*. 37(1), 149-163.

H. T. Song & T. Zhang. (2016). Fast robust integrated guidance and control design of interceptors, *IEEE Transactions on Control Systems Technology*. 24(1), 349-356.

M. C. Song, Y. Lin, & R. Huang. (2014). Robust adaptive dynamic surface control for linear time-varying systems, *International Journal of Adaptive Control and Signal Processing*. 28, 932-948.

C.L. Wang & Y. Lin. (2010). Adaptive dynamic surface control for linear multivariable systems, *Automatica*. 46(10), 1703-1711.

X. F. Wang, Y.Y. Zheng, & H. Lin. (2015). Integrated guidance and control law for cooperative attack of multiple missiles, *Aerospace Science and Technology*. 42, 1-11.

X. H. Wang, & J. Z. Wang. (2014). Partial integrated guidance and control for missiles with three-dimensional impact angle constraints, *Journal of Guidance Control and Dynamics*. 37(2), 644-657.

W.H. Wang, S.F. Xiong, S. Wang, S. Y. Song, & C. Lai. (2016). Three dimensional impact angle constrained integrated guidance and control for missiles with input saturation and actuator failure, *Aerospace Science and Technology*. 53, 169-187.

H.X. Wu, J. Hu, & Y.C. Xie. (2007). Characteristic model-based all-coefficient adaptive control method and its applications, *IEEE Transactions on Systems Man and Cybernetics Part C: Applications and Reviews*. 37(2), 213-221.

S. S. Vaddi, P. K. Menon, & E. J. Ohlmeyer. (2009). Numerical state-dependent Riccati equation approach for missile integrated guidance control, *Journal of Guidance Control and Dynamics*. 32(2), 699-703.

H. Yan & H.B. Ji. (2012). Integrated guidance and control for dual-control missiles based on small-gain theorem, *Automatica*. 48(10), 2686-2692.

H. Yan, X.H. Wang, B.F. Yu, & H.B. Ji. (2014). Adaptive integrated guidance and control based on backstepping and input-to-state stability, *Asian Journal of Control*. 16(2), 602-608.

C. Zhang & Y.J. Wu, (2016). Dynamic surface control and active disturbance rejection control-based integrated guidance and control design and simulation for hypersonic reentry missile, International *Journal of Modeling Simulation and Scientific Computing*. 7(3), 1650025.

Z. Zhang & J. Hu. (2012). Stability analysis of a hypersonic vehicle controlled by the characteristic model based adaptive controller, *Science China Information Sciences.* 55(10), 2243-2256.

9 NOTES ON CONTRIBUTORS

Jun Zhou received a Ph.D. in Navigation, Guidance and Control from Northwestern Polytechnical University, Xi'an, China in 1993. He is currently a professor at the School of Astronautics, Northwestern Polytechnical University, Xi'an, China. He is also the director of Institute of Precision Guidance and Control. His research interests include guidance and control systems of missiles and space vehicles, flight control and simulation technique, fault tolerance, and software engineering.

Zhenzhen Ge is a Ph.D. candidate from Institute of Precision Guidance and Control, at the School of Astronautics, Northwestern Polytechnical University, Xi'an, China. He received a M.Sc. in Navigation, Guidance and Control from Northwestern Polytechnical University in 2015. His main research interests include guidance and control of hypersonic vehicles, adaptive control and artificial intelligence.